The transverse momentum spectrum of weak gauge bosons at N^{3}LL+NNLO

Wojciech Bizoń[1,2], Aude Gehrmann-De Ridder[3,4], Thomas Gehrmann[4], Nigel Glover[5], Alexander Huss[6], Pier Francesco Monni[6], Emanuele Re[6,7], Luca Rottoli[8,9], and Duncan M. Walker[5]

1 Institut für Theoretische Teilchenphysik (TTP), KIT, 76128 Karlsruhe, Germany
2 Institut für Kernphysik (IKP), KIT, 76344 Eggenstein-Leopoldshafen, Germany
3 Institute for Theoretical Physics, ETH, CH-8093 Zürich, Switzerland
4 Department of Physics, University of Zürich, CH-8057 Zürich, Switzerland
5 Institute for Particle Physics Phenomenology, Durham University, Durham DH1 3LE, UK
6 CERN, Theoretical Physics Department, CH-1211 Geneva 23, Switzerland
7 LAPTh, Université Grenoble Alpes, Université Savoie Mont Blanc, CNRS, 74940 Annecy, France
8 Dipartimento di Fisica G. Occhialini, U2, Università degli Studi di Milano-Bicocca, Piazza della Scienza, 3, 20126 Milano, Italy
9 INFN, Sezione di Milano-Bicocca, 20126, Milano, Italy

Abstract. We present accurate QCD predictions for the transverse momentum ($p_\perp$) spectrum of electroweak gauge bosons at the LHC for 13 TeV collisions, based on a consistent combination of a NNLO calculation at large $p_\perp$ and N^{3}LL resummation in the small $p_\perp$ limit. The inclusion of higher order corrections leads to substantial changes in the shape of the differential distributions, and the residual perturbative uncertainties are reduced to the few percent level across the whole transverse momentum spectrum. We examine the ratio of $p_\perp$ distributions in charged- and neutral-current Drell-Yan production, and study different prescriptions for the estimate of perturbative uncertainties that rely on different degrees of correlation between these processes. We observe an excellent stability of the ratios with respect to the perturbative order, indicating a strong correlation between the corresponding QCD corrections.

1 Introduction

The differential spectrum of electroweak gauge bosons, measured via their leptonic decays, is among the most prominent observables at the LHC.

Owing to the outstanding precision of their experimental measurement [1–14], such observables allow for a precise extraction of some of the Standard Model (SM) parameters — such as the W boson mass [13], or parton densities [15–18] — as well as for the calibration of widely used event generators and analysis tools. For this reason, an accurate theoretical understanding of such observables is paramount to exploit the precise data and perform meticulous tests of the SM.

Inclusive and differential distributions for neutral and charged Drell-Yan (DY) production with lepton pair invariant mass M are nowadays known with very high precision. The total cross section is known fully differentially in the Born phase space up to NNLO [19–27], while differential distributions in transverse momentum $p_\perp$ were recently computed up to NNLO both for Z- [28–33] and W-boson [34–36] production. In the DY distributions, elec-

troweak corrections become important especially at large transverse momenta, and they have been computed to NLO accuracy in [37–40].

In kinematical regimes dominated by soft and collinear radiation, the fixed-order perturbative series for the differential $p_\perp$ distribution is affected by large logarithmic terms of the form $\alpha_s^n L^{2n-1}/p_\perp$, with $L \equiv \ln(M/p_\perp)$, which must be resummed to all orders for a reliable theoretical prediction. In such regimes, the perturbative (logarithmic) accuracy is defined in terms of the *logarithm* of the cumulative cross section Σ as

$$\ln(\Sigma(p_\perp)) \equiv \ln\left(\int_0^{p_\perp} dp'_\perp \frac{d\Sigma(p'_\perp)}{dp'_\perp}\right)$$
$$= \sum_n \left\{ \mathcal{O}\left(\alpha_s^n L^{n+1}\right) + \mathcal{O}\left(\alpha_s^n L^n\right) + \dots \right\}. \quad (1)$$

One refers to the dominant terms $\alpha_s^n L^{n+1}$ as leading logarithmic (LL), to terms $\alpha_s^n L^n$ as next-to-leading logarithmic (NLL), to $\alpha_s^n L^{n-1}$ as next-to-next-to-leading logarithmic (NNLL), and so on. The resummation of the $p_\perp$ spectrum of SM bosons has been studied in a multitude of theoretical formulations throughout the years [41–51], and

the current state of the art for phenomenological studies at the LHC reaches N³LL accuracy [51–54].

In this article, we reach a new milestone in the theoretical description of transverse momentum distributions in both neutral and charged DY production, aiming for percent level precision throughout the full kinematical range. This is achieved by matching the fixed-order NNLO QCD predictions with the N³LL resummation of large logarithmic corrections. We adopt the momentum-space formulation of refs. [49, 51], in which the resummation is performed by generating the QCD radiation by means of a Monte Carlo (MC) algorithm. All the necessary ingredients for the N³LL $p_\perp$ resummation have been computed in refs. [55–61]. The combined framework enables fully differential N³LL+NNLO predictions for distributions that take proper account of the fiducial volume definitions used in the experimental measurements.

The article is organised as follows. In section 2 we briefly review the computation of the NNLO differential distributions in DY-pair production with the parton-level code NNLOjet, as well as the resummation for the $p_\perp$ distributions using the computer program RadISH. Section 3 describes our results for 13 TeV LHC collisions. Finally, section 4 contains our conclusions.

2 Setup of the calculation

In this section we give a brief overview of the computational setup, and describe the ingredients of both the fixed order (Section 2.1) and the resummed (Section 2.2) calculations.

2.1 Fixed order

For the calculation of the DY process, we consider the off-shell production of either a pair of charged leptons (mediated by both a Z boson and a virtual photon) or a charged lepton and a neutrino (mediated by $W^\pm$ bosons), in association with partonic jets. The jet requirement is replaced by a lower cut on the transverse momentum of the pair, that acts as an infrared regulator of the fixed-order calculation, hence preventing the radiation from being entirely unresolved.

The NNLO QCD predictions for neutral and charged DY production have been obtained in refs. [28–36]. Relative to the LO distribution, in which the leptonic system recoils against a single parton, the NNLO calculation receives contributions from configurations with two extra partons (RR: double-real corrections [62–66]), with one extra parton and one extra loop (RV: real-virtual corrections [62,63,67–70]) and with no extra partons but two extra loops (VV: double-virtual corrections [71–74]). Each of the three contributions is separately infrared divergent either in an implicit manner from phase-space regions where the partonic radiation becomes unresolved (soft and/or collinear), or in a explicit manner from infrared poles in virtual loop corrections. Only the sum of the three contributions is finite.

We perform the calculation using the parton-level generator NNLOjet, which implements the antenna subtraction method [75–77] to isolate infrared singularities and to enable their cancellation between different contributions prior to the numerical phase-space integration. The NNLO calculation can be structured as

$$\sigma^{\mathrm{NNLO}}_{X+\mathrm{jet}} = \int_{\Phi_{X+3}} \left(\mathrm{d}\sigma^{RR}_{\mathrm{NNLO}} - \mathrm{d}\sigma^{S}_{\mathrm{NNLO}} \right)$$
$$+ \int_{\Phi_{X+2}} \left(\mathrm{d}\sigma^{RV}_{\mathrm{NNLO}} - \mathrm{d}\sigma^{T}_{\mathrm{NNLO}} \right)$$
$$+ \int_{\Phi_{X+1}} \left(\mathrm{d}\sigma^{VV}_{\mathrm{NNLO}} - \mathrm{d}\sigma^{U}_{\mathrm{NNLO}} \right). \quad (2)$$

The antenna subtraction terms, $\mathrm{d}\sigma^{S,T,U}_{\mathrm{NNLO}}$, are constructed from antenna functions [75, 78–82] to cancel infrared singularities between the contributions of different parton multiplicities. The integrals are performed over the phase space $\Phi_{X+1,2,3}$ corresponding to the production of the colour singlet in association with one, two or three partons in the final state. The integration over the final-state phase space is fully differential such that any infrared-safe observable $\mathcal{O}$ can be studied through differential distributions as $\mathrm{d}\sigma^{\mathrm{NNLO}}_{X+\mathrm{jet}}/\mathrm{d}\mathcal{O}$.

The matching of the above NNLO prediction to a resummed calculation in the small $p_\perp$ limit is computationally very challenging. At small $p_\perp$, both the matrix elements and the subtraction terms grow rapidly in magnitude due to the presence of un-cancelled infrared singularities. This results in large numerical cancellations between them that ultimately challenge the stability of the final prediction. The finite remainder of such cancellations needs to be numerically stable in order to be consistently combined with a resummed calculation and extrapolated to the limit $p_\perp \to 0$. The stability of NNLOjet in this extreme regime has been tested thoroughly against the expansion of the N³LL resummations in refs. [52,53], where it is shown that the NNLO calculation can be reliably obtained down to very small $p_\perp$ values.

The residual infrared (logarithmic) divergences that persist in the $p_\perp \to 0$ limit are cancelled by combining the fixed-order computation with a resummed calculation, where the logarithms in the fixed-order prediction are subtracted and replaced by the sum of the corresponding enhanced terms to all orders in perturbation theory. This procedure is discussed in the following Section 2.2.

2.2 Resummation and matching

The resummation is performed in momentum space by means of the method formulated in refs. [49, 51] and implemented in the computer code RadISH. In this approach, the factorisation properties of the QCD matrix elements in the soft and collinear limits are exploited to devise a numerical procedure to generate the radiation at all perturbative orders. This allows for the resummation of the large logarithmic terms in a fashion that is similar in spirit

to a Monte Carlo generator. A detailed technical description of the method can be found in Refs. [49, 51], and the formulae up to N³LL accuracy are collected in Ref. [53] (Section 3 and Appendix B).

In order to have a reliable prediction across the whole $p_\perp$ spectrum, the fixed-order and resummed predictions must be consistently combined through a matching procedure. The matching is performed in such a way that it reduces to the resummed calculation at small $p_\perp$, while reproducing the fixed-order prediction at large transverse momentum. At a given perturbative order, one can adopt various schemes that differ from one another by terms beyond the considered order. In the present analysis we adopt the multiplicative scheme formulated in refs. [53, 83], in which the matching is performed at the level of the cumulative distribution (1) as follows:

$$\Sigma_{\mathrm{match}}^{\mathrm{N^3LL}}(p_\perp) = \frac{\Sigma^{\mathrm{N^3LL}}(p_\perp)}{\Sigma_{\mathrm{asym.}}^{\mathrm{N^3LL}}} \left[\Sigma_{\mathrm{asym.}}^{\mathrm{N^3LL}} \frac{\Sigma^{\mathrm{N^3LO}}(p_\perp)}{\Sigma_{\mathrm{exp.}}^{\mathrm{N^3LL}}(p_\perp)} \right]_{\mathrm{N^3LO}}, \quad (3)$$

where $\Sigma_{\mathrm{exp.}}^{\mathrm{N^3LL}}$ denotes the expansion of the resummation formula $\Sigma^{\mathrm{N^3LL}}$ to $\mathcal{O}(\alpha_s^3)$ (N³LO), and the whole squared bracket in Eq. (3) is expanded to N³LO. It should be recalled that $\mathcal{O}(\alpha_s^3)$ corresponds to N³LO in the total (i.e. $p_\perp$-integrated) cross section and in any cumulative distribution, while being NNLO in the fixed-order $p_\perp$-differential cross section.

In the above equation, $\Sigma^{\mathrm{N^3LO}}$ is the cumulative fixed-order distribution at N³LO, i.e.

$$\Sigma^{\mathrm{N^3LO}}(p_\perp) = \sigma_{\mathrm{tot}}^{\mathrm{N^3LO}} - \int_{p_\perp}^{\infty} \mathrm{d}p'_\perp \, \frac{\mathrm{d}\Sigma^{\mathrm{NNLO}}(p'_\perp)}{\mathrm{d}p'_\perp}, \quad (4)$$

where $\sigma_{\mathrm{tot}}^{\mathrm{N^3LO}}$ is the total cross section for the charged or neutral DY processes at N³LO, and $\mathrm{d}\Sigma^{\mathrm{NNLO}}/\mathrm{d}p'_\perp$ denotes the corresponding NNLO $p_\perp$-differential distribution obtained with NNLOjet. Both of these quantities are accurate to $\mathcal{O}(\alpha_s^3)$. Since the N³LO inclusive cross section for DY production is currently unknown, we approximate it with the NNLO cross section [19–27] in the following. This approximation impacts only terms at N⁴LL order, and is thus beyond the accuracy considered in this study.

Finally, the quantity $\Sigma_{\mathrm{asym.}}^{\mathrm{N^3LL}}$ is defined as the asymptotic ($p_\perp \gg M$) limit of the resummed cross section

$$\Sigma^{\mathrm{N^3LL}}(p_\perp) \xrightarrow[p_\perp \gg M]{} \Sigma_{\mathrm{asym.}}^{\mathrm{N^3LL}}. \quad (5)$$

This prescription ensures that, in the $p_\perp \gg M$ limit, Eq. (3) reproduces by construction the fixed-order result, while in the $p_\perp \to 0$ limit it reduces to the resummed prediction. The detailed matching formulae can be found in Appendix A of ref. [53].

In the next section, we will also report matched predictions at lower perturbative orders, NNLL+NLO and NLL+LO, that are obtained from the following matched cumulative distributions

$$\Sigma_{\mathrm{match}}^{\mathrm{NNLL}}(p_\perp) = \frac{\Sigma^{\mathrm{NNLL}}(p_\perp)}{\Sigma_{\mathrm{asym.}}^{\mathrm{NNLL}}} \left[\Sigma_{\mathrm{asym.}}^{\mathrm{NNLL}} \frac{\Sigma^{\mathrm{NNLO}}(p_\perp)}{\Sigma_{\mathrm{exp.}}^{\mathrm{NNLL}}(p_\perp)} \right]_{\mathrm{NNLO}}, \quad (6)$$

$$\Sigma_{\mathrm{match}}^{\mathrm{NLL}}(p_\perp) = \frac{\Sigma^{\mathrm{NLL}}(p_\perp)}{\Sigma_{\mathrm{asym.}}^{\mathrm{NLL}}} \left[\Sigma_{\mathrm{asym.}}^{\mathrm{NLL}} \frac{\Sigma^{\mathrm{NLO}}(p_\perp)}{\Sigma_{\mathrm{exp.}}^{\mathrm{NLL}}(p_\perp)} \right]_{\mathrm{NLO}}. \quad (7)$$

The above matching schemes guarantee that in the large-$p_\perp$ limit the matched cumulative cross sections reproduce, by construction, the following total cross sections

$$\Sigma_{\mathrm{match}}^{\mathrm{N^3LL}}(p_\perp) \xrightarrow[p_\perp \gg M]{} \sigma_{\mathrm{tot}}^{\mathrm{NNLO}},$$
$$\Sigma_{\mathrm{match}}^{\mathrm{NNLL}}(p_\perp) \xrightarrow[p_\perp \gg M]{} \sigma_{\mathrm{tot}}^{\mathrm{NNLO}},$$
$$\Sigma_{\mathrm{match}}^{\mathrm{NLL}}(p_\perp) \xrightarrow[p_\perp \gg M]{} \sigma_{\mathrm{tot}}^{\mathrm{NLO}}. \quad (8)$$

We stress once more that the $\Sigma_{\mathrm{match}}^{\mathrm{N^3LL}}$ reproduces the NNLO total cross section at large $p_\perp$ since the N³LO result for the inclusive DY process is currently unknown. The nominal accuracy of the predictions is unaffected by this choice.

The final normalised distributions that will be reported in Section 3 are obtained by differentiating Eqs. (3), (6) and (7), and dividing by the respective total cross sections of the right hand side of Eq. (8).

We recall that the resummed calculation contains a Landau singularity arising from configurations where the radiation is generated with transverse momentum scales $k_\perp \sim M \exp\{-1/(2\beta_0\alpha_s)\}$ (with $\alpha_s = \alpha_s(M)$ and $\beta_0 = (11\,C_A - 2\,n_f)/(12\pi)$). In the predictions presented in the following, we set the results to zero when the hardest radiation's transverse momentum reaches the singularity. For the leptonic invariant masses studied here, this procedure acts on radiation emitted at very small transverse momentum that, due to the vectorial nature of the observable [41, 51], gives a very small contribution to the spectrum. We however stress that for a precise description of this kinematic regime, a thorough study of the impact of non-perturbative corrections is necessary.

3 Results at the LHC

In this section we report our numerical results for the neutral and charged DY transverse momentum distributions at N³LL+NNLO.

We consider pp collisions at a centre-of-mass energy of 13 TeV, and we use the NNLO NNPDF3.1 parton distribution function set [15] with $\alpha_s(M_Z) = 0.118$. The parton densities are evolved from a low scale $Q_0 \sim 1$ GeV forwards with LHAPDF [84], which correctly implements the heavy quark thresholds in the PDFs. All convolutions are handled with the Hoppet package [85]. In the results reported below, we use the NNLO DGLAP evolution of the adopted PDF set for all perturbative orders shown in the figures. Although the NNLO corrections to the PDF evolution are formally of order N³LL, we include them also in the NLL and NNLL predictions in order to guarantee a

consistent treatment of the quark thresholds in the parton densities. We note that this choice will lead to numerical differences in comparison to other NLL and NNLL results shown in the literature.

We adopt the G_μ scheme with the electro-weak parameters taken from the PDG [86], that is

$$M_Z = 91.1876 \text{ GeV}, \quad M_W = 80.379 \text{ GeV},$$
$$\Gamma_Z = 2.4952 \text{ GeV}, \quad \Gamma_W = 2.085 \text{ GeV},$$
$$G_F = 1.1663787 \times 10^{-5} \text{ GeV}^{-2}. \tag{9}$$

Moreover, we set the CKM matrix equal to the identity matrix, and we have verified that this approximation is accurate at the few-permille level. For both neutral-current and charged-current DY we apply fiducial selection cuts that resemble the ones used by ATLAS in previous analyses [4].

The final state for the neutral DY production is defined by applying the following set of fiducial selection cuts on the leptonic pair:

$$|\boldsymbol{p}_\perp^{\ell^\pm}| > 25 \text{ GeV}, \quad |\eta^{\ell^\pm}| < 2.5,$$
$$66 \text{ GeV} < M_{\ell\ell} < 116 \text{ GeV}, \tag{10}$$

where $\boldsymbol{p}_\perp^{\ell^\pm}$ are the transverse momenta of the two leptons, $\eta^{\ell^\pm}$ are their pseudo-rapidities in the hadronic centre-of-mass frame, and $M_{\ell\ell}$ is the invariant mass of the di-lepton system. The central factorisation and renormalisation scales are chosen to be $\mu_R = \mu_F = \sqrt{M_{\ell\ell}^2 + |\boldsymbol{p}_\perp^Z|^2}$ and the central resummation scale is set to $Q = M_{\ell\ell}/2$.

In the case of charged DY production, the fiducial volume is defined as

$$|\boldsymbol{p}_\perp^\ell| > 25 \text{ GeV}, \quad |\boldsymbol{E}\!\!\!/_T| > 25 \text{ GeV},$$
$$|\eta^\ell| < 2.5, \quad m_T > 50 \text{ GeV}, \tag{11}$$

where $\boldsymbol{E}\!\!\!/_T$ is the missing transverse energy vector and

$$m_T = \sqrt{\left(|\boldsymbol{p}_\perp^\ell| + |\boldsymbol{E}\!\!\!/_T|\right)^2 - \left(|\boldsymbol{p}_\perp^\ell + \boldsymbol{E}\!\!\!/_T|\right)^2}. \tag{12}$$

The central factorisation and renormalisation scales are chosen to be $\mu_R = \mu_F = \sqrt{M_{\ell\nu}^2 + |\boldsymbol{p}_\perp^W|^2}$ and the central resummation scale is again set to $Q = M_{\ell\nu}/2$.

In both processes, we assess the missing higher-order uncertainties by performing a variation of the renormalisation and factorisation scales by a factor of two around their respective central values whilst keeping $1/2 \leq \mu_R/\mu_F \leq 2$. In addition, for central factorisation and renormalisation scales, we vary the resummation scale Q by a factor of two in either direction. The final uncertainty is built as the envelope of the resulting nine-scale variation.

3.1 Fiducial distributions

We start by showing, in Figure 1, the comparison of the Z and $W^\pm$ normalised distributions at NLL+LO (green),

NNLL+NLO (blue), and N³LL+NNLO (red) in the fiducial volumes defined above. The lower inset of each panel of Figure 1 shows the ratio of all predictions to the previous state of the art (NNLL+NLO), with the same colour code as in the main panels. The difference between each prediction and the next order is of $\mathcal{O}(\alpha_s)$, both in the large $p_\perp$ region and in the limit $p_\perp \to 0$ where $\alpha_s L \sim 1$.

In comparison to the NNLL+NLO result, we note that the N³LL+NNLO corrections lead to important distortions in the shape of the distributions, making the spectrum harder for $p_\perp \gtrsim 10$ GeV, and softer below this scale. The perturbative errors are reduced by more than a factor of two across the whole $p_\perp$ range, and the leftover uncertainty is at the 5% level. In general, we observe a good convergence of the perturbative description when the order is increased, although in some $p_\perp$ regions the N³LL+NNLO and the NNLL+NLO bands overlap only marginally. This feature can be understood by noticing that, as mentioned in Section 2.2, both predictions are normalised to the same NNLO total cross section. Since at large $p_\perp$ the NNLO corrections lead to an increase in the spectrum of about 10%, by unitarity of the matching procedure (that preserves the total cross section) this must be balanced by an analogous decrease in the spectrum in the region governed by resummation, as indeed observed in Figure 1. We stress, nevertheless, that the two orders are compatible within the quoted uncertainties.

In Figure 2, we show the comparison among the NNLO (green), the NNLL+NLO (blue), and N³LL+NNLO (red) predictions, where the bands are obtained as discussed above. Alongside these results, we also show the Monte Carlo predictions obtained using the `Pythia8` generator [87] with the `AZ` tune [3], that has been obtained from the Z-boson $p_\perp$ distribution at 7 TeV. At 7 TeV and 8 TeV the above tune is known to correctly describe the Z transverse momentum spectrum within a few percent for $p_\perp \lesssim 50$ GeV [3], and it has been employed in the extraction of the W-boson mass by the ATLAS collaboration [13]. Although it is currently unknown how this tune performs at 13 TeV in comparison to the data, we use the `Pythia8` prediction for reference in the following plots. In particular, the lower inset of each panel of Figure 2 shows the ratio of all predictions to `Pythia8`. We observe a reasonable agreement between the N³LL+NNLO predictions and `Pythia8` below 30 GeV, while it deteriorates for larger $p_\perp$ values. This feature is particularly visible in the case of $W^\pm$ production.

A comparison of the N³LL+NNLO band to the fixed-order one shows that the resummation starts making a significant difference for $p_\perp \lesssim 20$ GeV, while above this scale the NNLO provides a reliable theoretical prediction. To further quantify the relative impact of the non-singular contributions in this region, we show in Fig. 3 the difference

$$\Delta^{\text{N}^3\text{LL}} \equiv (\, \mathrm{d}\Sigma^{\text{N}^3\text{LL+NNLO}}/\mathrm{d}p_\perp - \mathrm{d}\Sigma^{\text{N}^3\text{LL}}/\mathrm{d}p_\perp)/\sigma_{\text{tot}}^{\text{NNLO}} \tag{13}$$

between the matched and the resummed predictions for the Z and $W^\pm$ normalised distributions. In the lower panel of the plot we show the relative size
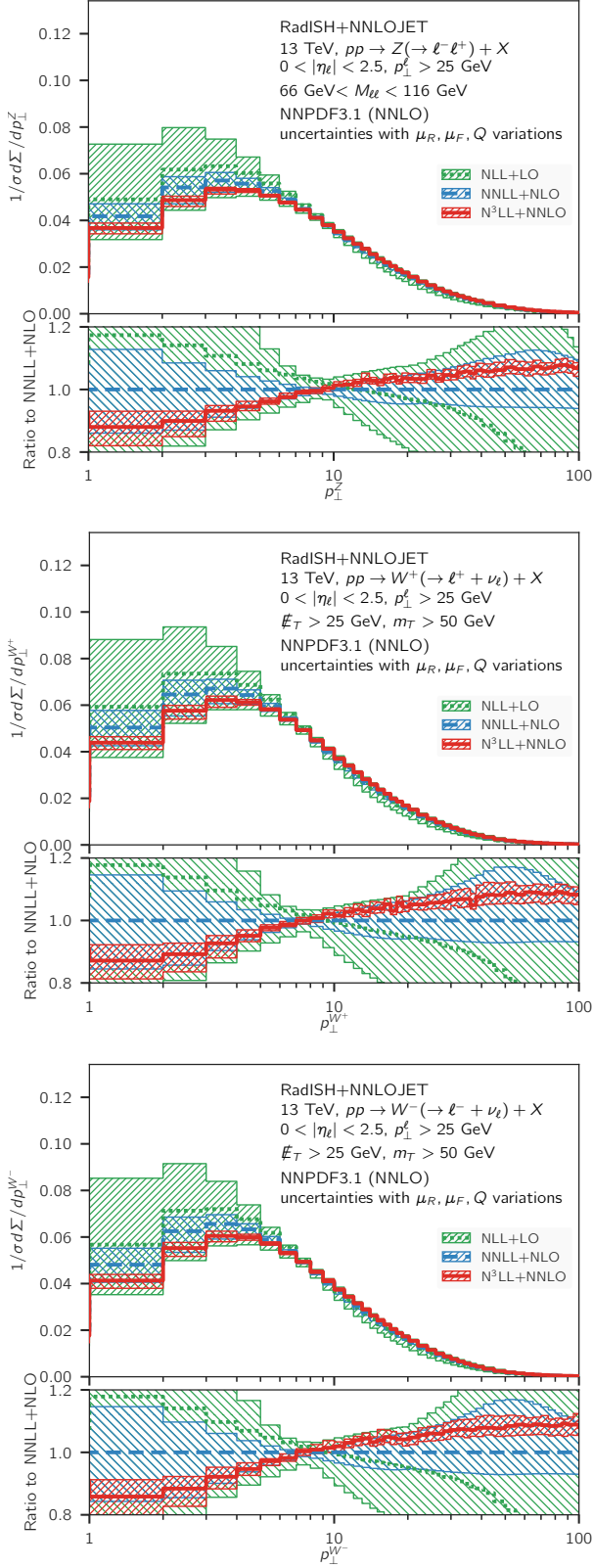
Fig. 1. Comparison of the normalised transverse momentum distribution for neutral and charged Drell-Yan pair production at NLL+LO (green, dotted), NNLL+NLO (blue, dashed) and N³LL+NNLO (red, solid) at $\sqrt{s} = 13$ TeV for the fiducial volume defined in the text. The lower panel shows the ratio to the NNLL+NLO result.
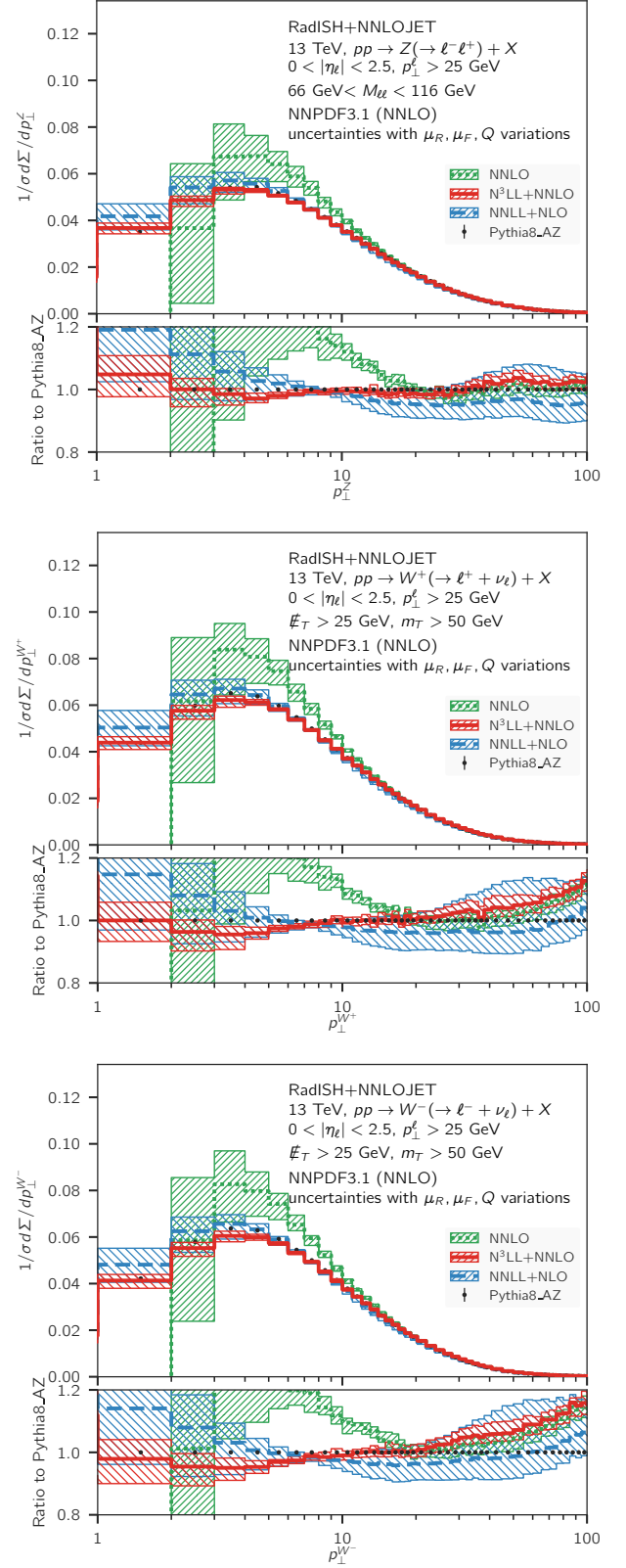
Fig. 2. Comparison of the normalised transverse momentum distribution for neutral and charged Drell-Yan pair production at NNLO (green, dotted), NNLL+NLO (blue, dashed) and N³LL+NNLO (red, solid) at $\sqrt{s} = 13$ TeV for the fiducial volume defined in the text. For reference, the `Pythia8` prediction in the `AZ` tune is also shown, and the lower panel shows the ratio of each prediction to the `Pythia8` result.

of $\Delta^{\mathrm{N^3LL}}$ with respect to the matched N³LL+NNLO result, $\Delta^{\mathrm{N^3LL}}/(\Sigma^{\mathrm{N^3LL+NNLO}}/\mathrm{d}p_\perp/\sigma^{\mathrm{NNLO}}_{\mathrm{tot}})$. The non-singular contributions are somewhat larger for $W^\pm$; the relative size of $\Delta^{\mathrm{N^3LL}}$ with respect to the N³LL+NNLO result is smaller than 5% (10%) for Z ($W^\pm$) for $p_\perp \lesssim$ 10 GeV, and becomes larger than 10% (20%) for $p_\perp >$ 20 GeV.
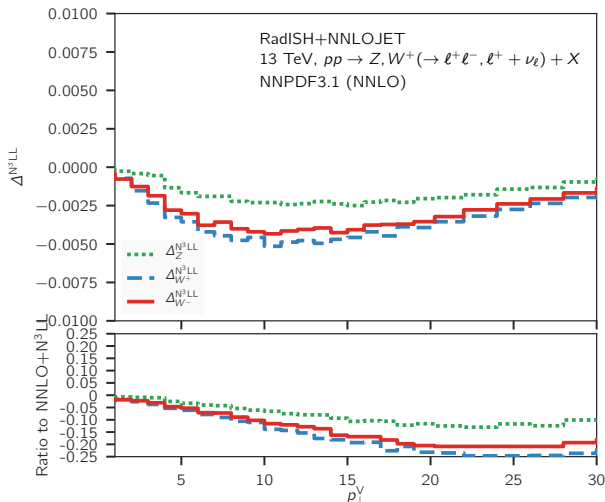
Fig. 3. Difference eq. (13) between the matched and the resummed predictions for the Z (green, dotted), W^+ (blue, dashed) and W^- (red, solid) normalised distributions. The lower panel shows the ratio of $\Delta^{\mathrm{N^3LL}}$ to the N³LL+NNLO matched result.

3.2 Ratio of Z/W and W^-/W^+ distributions

Another set of important quantities of interest are the ratios of the above distributions, which play a central role in recent extractions of the W-boson mass at the LHC [13]. When taking ratios of perturbative quantities one has to decide how to combine the uncertainties in the numerator and denominator to obtain the final error.

One option is to try to identify the possible sources of correlation in the three processes considered here. From the point of view of the perturbative (massless) QCD description adopted in this study, one expects the structure of radiative corrections to such reactions to be nearly identical. This is certainly the case as far as resummation is concerned, since it is governed by the same anomalous dimensions and all-order structure in W and Z production. As a consequence, the resummation scale should be varied in a correlated manner in both predictions considered in the ratio. A similar argument can be made regarding the renormalisation scale μ_R and the factorisation scale μ_F.

However, an important difference between Z, W^+, and W^- production lies in the different combination of partonic channels probed by each process and, in particular, in the sensitivity to different heavy quark thresholds in

the PDFs at small $p_\perp$. Therefore, it is not clear whether a fully correlated variation of the factorisation scale μ_F is physically justified. A more conservative uncertainty prescription is to vary the scales μ_R and Q in numerator and denominator in a fully correlated way, while varying μ_F in an uncorrelated manner within the constraint [36]

$$\frac{1}{2} \le \frac{x^{\mathrm{num.}}_{\mu_F}}{x^{\mathrm{den.}}_{\mu_F}} \le 2 \,, \qquad (14)$$

where x_{μ_F} is the ratio of the factorisation scale to its central value. This corresponds to a total of 17 scale combinations.

Finally, for comparison we also consider the uncorrelated variation of μ_R and μ_F in the ratio, while imposing

$$\frac{1}{2} \le \frac{x^{\mathrm{num.}}_{\mu}}{x^{\mathrm{den.}}_{\mu}} \le 2 \,, \qquad (15)$$

where x_μ is the ratio of the scale μ to its central value, with $\mu \equiv \{\mu_R, \mu_F\}$, together with a correlated variation of the resummation scale Q. This recipe amounts to taking the envelope of the predictions resulting from 33 different combinations of scales in the ratio.

To examine the reliability of the above uncertainty schemes, in Figure 4 we analyse the convergence of the perturbative series for the ratios of distributions, by comparing the results at NLL+LO (green), NNLL+NLO (blue), and N³LL+NNLO (red). The three lower panels in each plot show the theory uncertainties obtained according to the three prescriptions outlined above, respectively, in comparison to the old state-of-the-art prediction at NNLL+NLO. In the case of the Z/W^+ ratio (shown in the upper plot of Figure 4), we observe that the different perturbative orders are very close to one another. The results are compatible even within the uncertainty bands obtained with the more aggressive error estimate, which in some bins is sensitive to minor statistical fluctuations due to the complexity of the NNLO calculation. This feature is strikingly evident in the case of the W^-/W^+ ratio (lower figure), where the excellent convergence of the series seems to indicate that either a fully correlated scale variation or the more conservative estimate of Eq. (14) is perfectly justified.

Figure 5 shows the comparison of the same two ratios (Z/W^+ and W^-/W^+) to the NNLO result (green), and to Pythia8. We observe that in both cases the N³LL+NNLO calculation leads to an important reduction of the theory uncertainty. In particular, even with the most conservative estimate of the theory error, our best prediction leads to errors of the order of 5%, with the exception of the first bin where the perturbative uncertainty is at the 10% level. The kink around $p_\perp \sim 50 - 60$ GeV in the Z/W^+ ratio (upper plot in Figure 5) is due to the different fiducial selection cuts in the two processes. A change in the shape of the distributions around this scale is indeed visible in Figure 2, at slightly different $p_\perp$ values for Z and W^+ production, respectively, that is reflected in the structure observed in Figure 5. We find a good agreement between our best predictions at N³LL+NNLO and the Pythia8
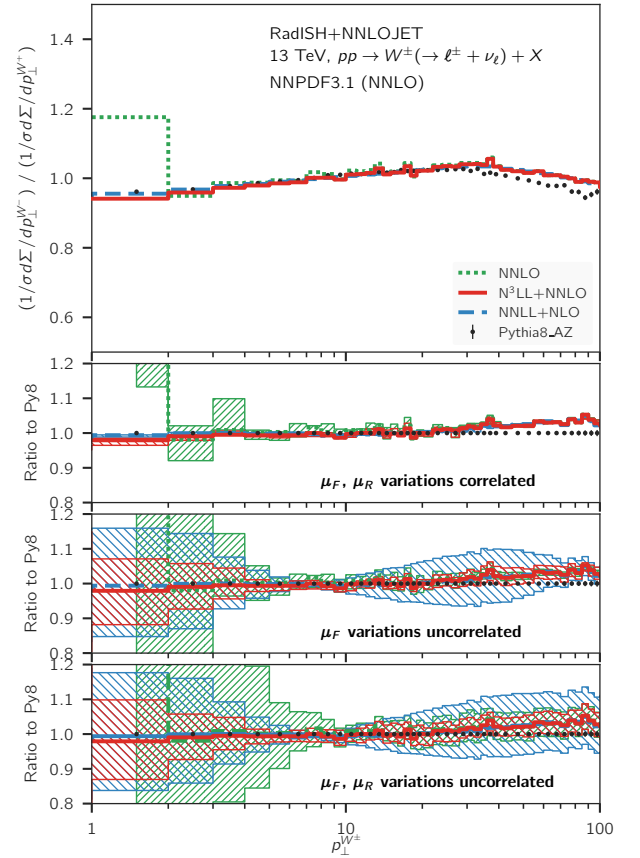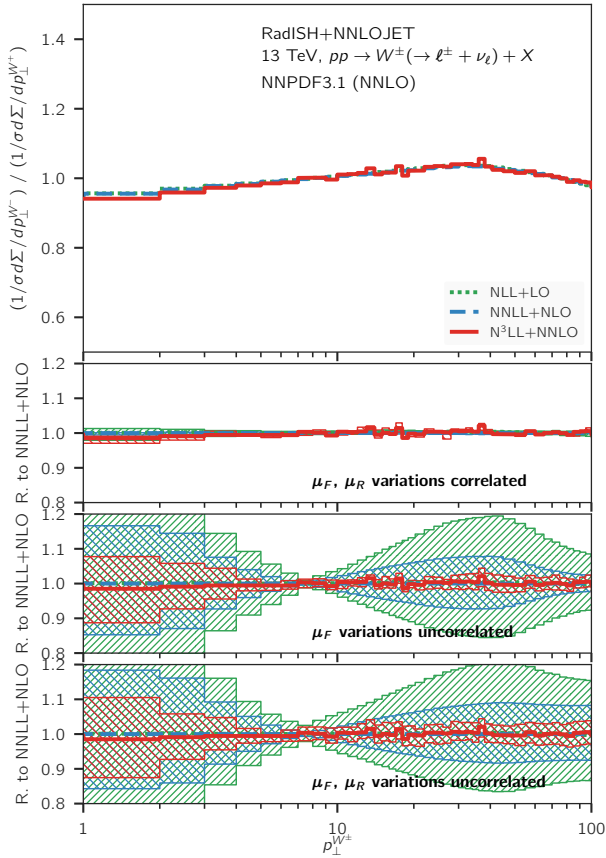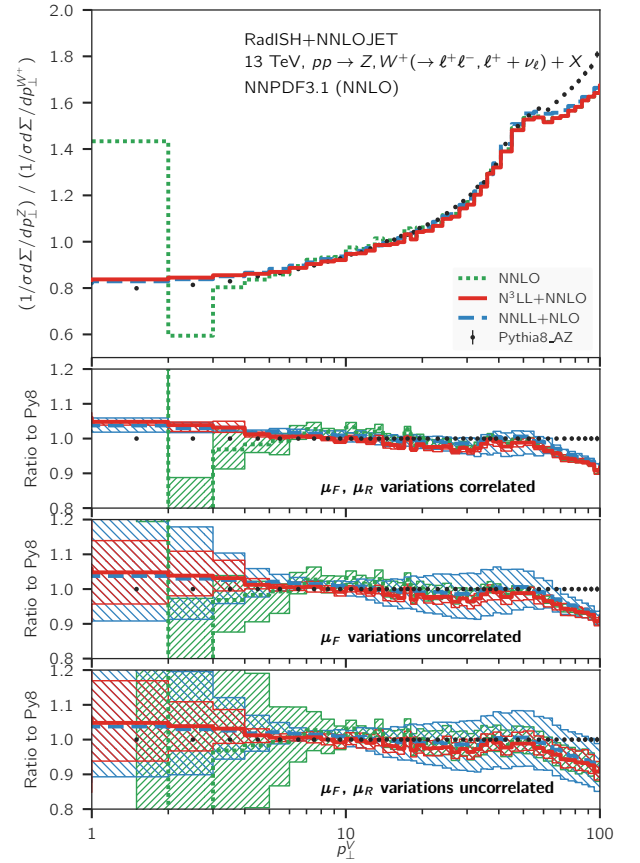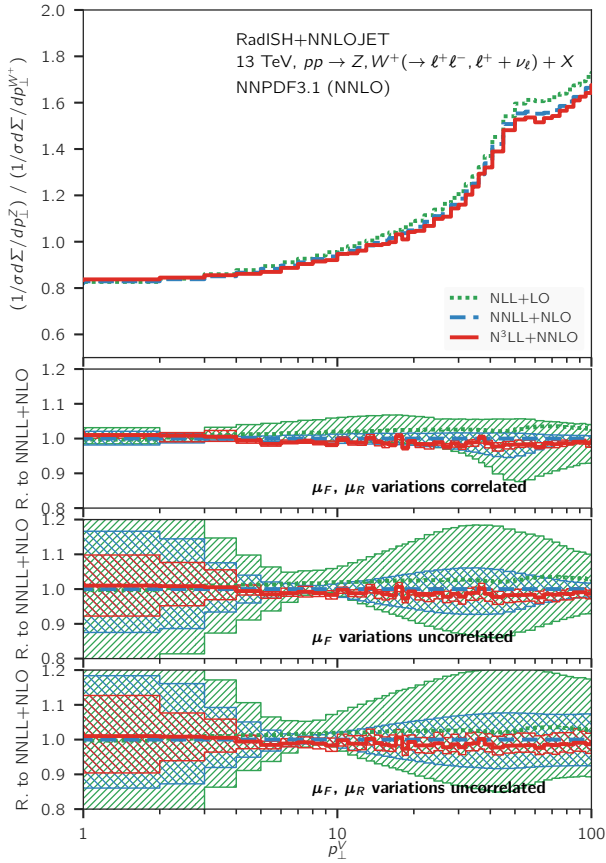
Fig. 4. Ratios of Z/W^+ and W^-/W^+ normalised differential distributions at NLL+LO (green, dotted), NNLL+NLO (blue, dashed) and N³LL+NNLO (red, solid) at $\sqrt{s} = 13$ TeV. The three lower panels show three different prescriptions for the theory uncertainty, as described in the text.

Fig. 5. Ratios of Z/W^+ and W^-/W^+ normalised differential distributions at NNLO (green, dotted), NNLL+NLO (blue, dashed) and N³LL+NNLO (red, solid) at $\sqrt{s} = 13$ TeV. For reference, the `Pythia8` prediction in the `AZ` tune is also shown, and the lower panels show the ratio of each prediction to the latter.

Monte Carlo in the small $p_\perp$ region of the ratios. However, the two predictions are not compatible within the quoted theory uncertainties if the scales are varied in a fully correlated manner. On the other hand, for $p_\perp \gtrsim 40$ GeV, the Pythia8 result disagrees with the matched calculation. This behavior is not unexpected, since the nominal perturbative accuracy of Pythia8 is well below any of the matched calculations, and the AZ tune is optimised to describe the Z spectrum in the region $p_\perp \leq 50$ GeV at 7 TeV.

4 Conclusions

In this work, we computed the transverse momentum distributions of electroweak gauge bosons at the LHC to N^{3}LL+NNLO accuracy in QCD. This calculation opens up a new level of theoretical precision in the description of these observables. The new state-of-the-art prediction is obtained by combining the NNLO results from the NNLOjet program with the N^{3}LL resummation performed with RadISH. Our phenomenological study adopts fiducial selection cuts similar to the setup adopted by ATLAS in previous studies. The numerical results we presented are made available in electronic format as additional material alongside this manuscript.

We find that, in comparison to the fixed-order prediction, the resummation effects become important for $p_\perp \lesssim 20$ GeV. The effect of the N^{3}LL+NNLO corrections with respect to the previous NNLL+NLO prediction is as large as $\sim 10\%$, and leads to significant shape distortions as well as to a substantial reduction in the perturbative uncertainty due to missing higher-order corrections. In particular, the distributions considered in this article are predicted with a residual uncertainty below the 5% level across most of the $p_\perp$ spectrum. We also compared the results to the predictions obtained from the Pythia8 Monte Carlo with the AZ tune, that has been determined using the ATLAS experimental data for the Z boson transverse momentum at 7 TeV [3].

Finally, we examined the ratios of the Z to W^+, and W^- to W^+ distributions, which play an important role in the W mass extraction at the LHC. We consider different prescriptions for the estimate of perturbative uncertainties that rely on different degrees of correlation between the scales in the numerator and in the denominator. We find a remarkable convergence of the predictions for the ratios at different perturbative orders. This fact strongly indicates that the class of processes considered in this study feature very similar perturbative corrections suggesting that the perturbative sources of uncertainty are correlated to a large extent.

There are, however, additional sources of perturbative corrections to $W^\pm$ and Z production that we ignored in our study. In particular, at the level of the residual theoretical errors obtained in our predictions, PDF theory uncertainties [88, 89], QED corrections [90, 91], as well as a careful study of the impact of mass effects [92–102] become necessary. The correlation pattern between the uncertainties due to such effects may well be different from what we have observed in this paper, and a dedicated study must be performed in order to reliably combine these effects with the N^{3}LL+NNLO predictions presented here.

References

1. S. Chatrchyan, et al., Phys. Rev. **D85**, 032002 (2012), 1110.4973
2. G. Aad, et al., Phys. Lett. **B720**, 32 (2013), 1211.6899
3. G. Aad, et al., JHEP **09**, 145 (2014), 1406.3660
4. G. Aad, et al., Eur. Phys. J. **C76**(5), 291 (2016), 1512.02192
5. R. Aaij, et al., JHEP **08**, 039 (2015), 1505.07024
6. V. Khachatryan, et al., Phys. Lett. **B749**, 187 (2015), 1504.03511
7. V. Khachatryan, et al., Phys. Lett. **B750**, 154 (2015), 1504.03512
8. R. Aaij, et al., JHEP **01**, 155 (2016), 1511.08039
9. G. Aad, et al., JHEP **08**, 159 (2016), 1606.00689
10. V. Khachatryan, et al., JHEP **02**, 096 (2017), 1606.05864
11. R. Aaij, et al., JHEP **09**, 136 (2016), 1607.06495
12. A.M. Sirunyan, et al., JHEP **03**, 172 (2018), 1710.07955
13. M. Aaboud, et al., Eur. Phys. J. **C78**(2), 110 (2018), 1701.07240
14. M. Aaboud, et al., JHEP **12**, 059 (2017), 1710.05167
15. R.D. Ball, et al., Eur. Phys. J. **C77**(10), 663 (2017), 1706.00428
16. R. Boughezal, A. Guffanti, F. Petriello, M. Ubiali, JHEP **07**, 130 (2017), 1705.00343
17. A. Bacchetta, F. Delcarro, C. Pisano, M. Radici, A. Signori, JHEP **06**, 081 (2017), 1703.10157
18. V. Bertone, I. Scimemi, A. Vladimirov, (2019), 1902.08474
19. R. Hamberg, W.L. van Neerven, T. Matsuura, Nucl. Phys. **B359**, 343 (1991). [Erratum: Nucl. Phys.B644,403(2002)]

20. W.L. van Neerven, E.B. Zijlstra, Nucl. Phys. **B382**, 11 (1992). [Erratum: Nucl. Phys.B680,513(2004)]
21. C. Anastasiou, L.J. Dixon, K. Melnikov, F. Petriello, Phys. Rev. Lett. **91**, 182002 (2003), hep-ph/0306192
22. K. Melnikov, F. Petriello, Phys. Rev. Lett. **96**, 231803 (2006), hep-ph/0603182
23. K. Melnikov, F. Petriello, Phys. Rev. **D74**, 114017 (2006), hep-ph/0609070
24. S. Catani, G. Ferrera, M. Grazzini, JHEP **05**, 006 (2010), 1002.3115
25. S. Catani, L. Cieri, G. Ferrera, D. de Florian, M. Grazzini, Phys. Rev. Lett. **103**, 082001 (2009), 0903.2120
26. R. Gavin, Y. Li, F. Petriello, S. Quackenbush, Comput. Phys. Commun. **182**, 2388 (2011), 1011.3540
27. C. Anastasiou, L.J. Dixon, K. Melnikov, F. Petriello, Phys. Rev. **D69**, 094008 (2004), hep-ph/0312266
28. A. Gehrmann-De Ridder, T. Gehrmann, E.W.N. Glover, A. Huss, T.A. Morgan, Phys. Rev. Lett. **117**(2), 022001 (2016), 1507.02850
29. A. Gehrmann-De Ridder, T. Gehrmann, E.W.N. Glover, A. Huss, T.A. Morgan, JHEP **07**, 133 (2016), 1605.04295
30. A. Gehrmann-De Ridder, T. Gehrmann, E.W.N. Glover, A. Huss, T.A. Morgan, JHEP **11**, 094 (2016), 1610.01843
31. R. Gauld, A. Gehrmann-De Ridder, T. Gehrmann, E.W.N. Glover, A. Huss, JHEP **11**, 003 (2017), 1708.00008
32. R. Boughezal, J.M. Campbell, R.K. Ellis, C. Focke, W.T. Giele, X. Liu, F. Petriello, Phys. Rev. Lett. **116**(15), 152001 (2016), 1512.01291
33. R. Boughezal, X. Liu, F. Petriello, Phys. Rev. **D94**(7), 074015 (2016), 1602.08140
34. R. Boughezal, C. Focke, X. Liu, F. Petriello, Phys. Rev. Lett. **115**(6), 062002 (2015), 1504.02131
35. R. Boughezal, X. Liu, F. Petriello, Phys. Rev. **D94**(11), 113009 (2016), 1602.06965
36. A. Gehrmann-De Ridder, T. Gehrmann, E.W.N. Glover, A. Huss, D.M. Walker, Phys. Rev. Lett. **120**(12), 122001 (2018), 1712.07543
37. J.H. Kühn, A. Kulesza, S. Pozzorini, M. Schulze, Nucl. Phys. **B727**, 368 (2005), hep-ph/0507178
38. J.H. Kühn, A. Kulesza, S. Pozzorini, M. Schulze, Phys. Lett. **B651**, 160 (2007), hep-ph/0703283
39. A. Denner, S. Dittmaier, T. Kasprzik, A. Mück, JHEP **08**, 075 (2009), 0906.1656
40. A. Denner, S. Dittmaier, T. Kasprzik, A. Mück, JHEP **06**, 069 (2011), 1103.0914
41. G. Parisi, R. Petronzio, Nucl. Phys. **B154**, 427 (1979)
42. J.C. Collins, D.E. Soper, G.F. Sterman, Nucl. Phys. **B250**, 199 (1985)
43. C. Balazs, C.P. Yuan, Phys. Rev. **D56**, 5558 (1997), hep-ph/9704258
44. F. Landry, R. Brock, P.M. Nadolsky, C.P. Yuan, Phys. Rev. **D67**, 073016 (2003), hep-ph/0212159
45. T. Becher, M. Neubert, Eur. Phys. J. **C71**, 1665 (2011), 1007.4005
46. G. Bozzi, S. Catani, G. Ferrera, D. de Florian, M. Grazzini, Phys. Lett. **B696**, 207 (2011), 1007.2351
47. T. Becher, M. Neubert, D. Wilhelm, JHEP **02**, 124 (2012), 1109.6027
48. M.G. Echevarria, A. Idilbi, I. Scimemi, JHEP **07**, 002 (2012), 1111.4996
49. P.F. Monni, E. Re, P. Torrielli, Phys. Rev. Lett. **116**(24), 242001 (2016), 1604.02191
50. M.A. Ebert, F.J. Tackmann, JHEP **02**, 110 (2017), 1611.08610
51. W. Bizon, P.F. Monni, E. Re, L. Rottoli, P. Torrielli, JHEP **02**, 108 (2018), 1705.09127
52. X. Chen, T. Gehrmann, E.W.N. Glover, A. Huss, Y. Li, D. Neill, M. Schulze, I.W. Stewart, H.X. Zhu, Phys. Lett. **B788**, 425 (2019), 1805.00736
53. W. Bizoń, X. Chen, A. Gehrmann-De Ridder, T. Gehrmann, N. Glover, A. Huss, P.F. Monni, E. Re, L. Rottoli, P. Torrielli, JHEP **12**, 132 (2018), 1805.05916
54. T. Becher, M. Hager, (2019), 1904.08325
55. S. Catani, L. Cieri, D. de Florian, G. Ferrera, M. Grazzini, Eur. Phys. J. **C72**, 2195 (2012), 1209.0158
56. T. Gehrmann, T. Lübbert, L.L. Yang, JHEP **06**, 155 (2014), 1403.6451
57. M.G. Echevarria, I. Scimemi, A. Vladimirov, JHEP **09**, 004 (2016), 1604.07869
58. Y. Li, H.X. Zhu, Phys. Rev. Lett. **118**(2), 022004 (2017), 1604.01404
59. A.A. Vladimirov, Phys. Rev. Lett. **118**(6), 062001 (2017), 1610.05791
60. S. Moch, B. Ruijl, T. Ueda, J.A.M. Vermaseren, A. Vogt, Phys. Lett. **B782**, 627 (2018), 1805.09638
61. R.N. Lee, A.V. Smirnov, V.A. Smirnov, M. Steinhauser, JHEP **02**, 172 (2019), 1901.02898
62. J.M. Campbell, R.K. Ellis, Phys. Rev. **D65**, 113007 (2002), hep-ph/0202176
63. J.M. Campbell, R.K. Ellis, D.L. Rainwater, Phys. Rev. **D68**, 094021 (2003), hep-ph/0308195
64. K. Hagiwara, D. Zeppenfeld, Nucl. Phys. **B313**, 560 (1989)
65. F.A. Berends, W.T. Giele, H. Kuijf, Nucl. Phys. **B321**, 39 (1989)
66. N.K. Falck, D. Graudenz, G. Kramer, Nucl. Phys. **B328**, 317 (1989)
67. E.W.N. Glover, D.J. Miller, Phys. Lett. **B396**, 257 (1997), hep-ph/9609474
68. Z. Bern, L.J. Dixon, D.A. Kosower, S. Weinzierl, Nucl. Phys. **B489**, 3 (1997), hep-ph/9610370
69. J.M. Campbell, E.W.N. Glover, D.J. Miller, Phys. Lett. **B409**, 503 (1997), hep-ph/9706297
70. Z. Bern, L.J. Dixon, D.A. Kosower, Nucl. Phys. **B513**, 3 (1998), hep-ph/9708239
71. S. Moch, P. Uwer, S. Weinzierl, Phys. Rev. **D66**, 114001 (2002), hep-ph/0207043
72. L.W. Garland, T. Gehrmann, E.W.N. Glover, A. Koukoutsakis, E. Remiddi, Nucl. Phys. **B627**, 107 (2002), hep-ph/0112081
73. L.W. Garland, T. Gehrmann, E.W.N. Glover, A. Koukoutsakis, E. Remiddi, Nucl. Phys. **B642**, 227 (2002), hep-ph/0206067
74. T. Gehrmann, L. Tancredi, JHEP **02**, 004 (2012), 1112.1531
75. A. Gehrmann-De Ridder, T. Gehrmann, E.W.N. Glover, JHEP **0509**, 056 (2005), hep-ph/0505111
76. A. Daleo, T. Gehrmann, D. Maitre, JHEP **04**, 016 (2007), hep-ph/0612257
77. J. Currie, E.W.N. Glover, S. Wells, JHEP **04**, 066 (2013), 1301.4693
78. A. Gehrmann-De Ridder, T. Gehrmann, E.W.N. Glover, Phys. Lett. **B612**, 49 (2005), hep-ph/0502110
79. A. Daleo, A. Gehrmann-De Ridder, T. Gehrmann, G. Luisoni, JHEP **1001**, 118 (2010), 0912.0374

80. R. Boughezal, A. Gehrmann-De Ridder, M. Ritzmann, JHEP **02**, 098 (2011), 1011.6631
81. T. Gehrmann, P.F. Monni, JHEP **12**, 049 (2011), 1107.4037
82. A. Gehrmann-De Ridder, T. Gehrmann, M. Ritzmann, JHEP **10**, 047 (2012), 1207.5779
83. F. Caola, J.M. Lindert, K. Melnikov, P.F. Monni, L. Tancredi, C. Wever, JHEP **09**, 035 (2018), 1804.07632
84. A. Buckley, J. Ferrando, S. Lloyd, K. Nordström, B. Page, M. Rüfenacht, M. Schönherr, G. Watt, Eur. Phys. J. **C75**, 132 (2015), 1412.7420
85. G.P. Salam, J. Rojo, Comput. Phys. Commun. **180**, 120 (2009), 0804.3755
86. M. Tanabashi, et al., Phys. Rev. **D98**(3), 030001 (2018)
87. T. Sjöstrand, S. Ask, J.R. Christiansen, R. Corke, N. Desai, P. Ilten, S. Mrenna, S. Prestel, C.O. Rasmussen, P.Z. Skands, Comput. Phys. Commun. **191**, 159 (2015), 1410.3012
88. L.A. Harland-Lang, R.S. Thorne, Eur. Phys. J. **C79**(3), 225 (2019), 1811.08434
89. R. Abdul Khalek, et al., Eur. Phys. J. **C79**, 838 (2019), 1905.04311
90. D. de Florian, M. Der, I. Fabre, Phys. Rev. **D98**(9), 094008 (2018), 1805.12214
91. L. Cieri, G. Ferrera, G.F.R. Sborlini, JHEP **08**, 165 (2018), 1805.11948
92. M.A.G. Aivazis, J.C. Collins, F.I. Olness, W.K. Tung, Phys. Rev. **D50**, 3102 (1994), hep-ph/9312319
93. R.S. Thorne, R.G. Roberts, Phys. Rev. **D57**, 6871 (1998), hep-ph/9709442
94. J.C. Collins, Phys. Rev. **D58**, 094002 (1998), hep-ph/9806259
95. S. Berge, P.M. Nadolsky, F.I. Olness, Phys. Rev. **D73**, 013002 (2006), hep-ph/0509023
96. S. Forte, E. Laenen, P. Nason, J. Rojo, Nucl. Phys. **B834**, 116 (2010), 1001.2312
97. P. Pietrulewicz, D. Samitz, A. Spiering, F.J. Tackmann, JHEP **08**, 114 (2017), 1703.09702
98. C.M. Carloni Calame, M. Chiesa, H. Martinez, G. Montagna, O. Nicrosini, F. Piccinini, A. Vicini, Phys. Rev. **D96**(9), 093005 (2017), 1612.02841
99. F. Krauss, D. Napoletano, Phys. Rev. **D98**(9), 096002 (2018), 1712.06832
100. D. Figueroa, S. Honeywell, S. Quackenbush, L. Reina, C. Reuschle, D. Wackeroth, Phys. Rev. **D98**(9), 093002 (2018), 1805.01353
101. S. Forte, D. Napoletano, M. Ubiali, Eur. Phys. J. **C78**(11), 932 (2018), 1803.10248
102. E. Bagnaschi, F. Maltoni, A. Vicini, M. Zaro, JHEP **07**, 101 (2018), 1803.04336